GEOPHYSICS

Coupled afterslip and transient mantle flow after the 2011 Tohoku earthquake

J. Muto[1]*, J. D. P. Moore[2]*, S. Barbot[2,3], T. Iinuma[4], Y. Ohta[5], H. Iwamori[6,7,8]

Modeling of postseismic deformation following great earthquakes has revealed the viscous structure of the mantle and the frictional properties of the fault interface. However, for giant megathrust events, viscoelastic flow and afterslip mechanically interplay with each other during the postseismic period. We explore the role of afterslip and viscoelastic relaxation and their interaction in the aftermath of the 2011 M_w (moment magnitude) 9.0 Tohoku earthquake based on a detailed model analysis of the postseismic deformation with laterally varying, experimentally constrained, rock rheology. Mechanical coupling between viscoelastic relaxation and afterslip notably modifies both the afterslip distribution and surface deformation. Thus, we highlight the importance of addressing mechanical coupling for long-term studies of postseismic relaxation, especially in the context of the geodynamics of the Japan trench across the seismic cycle.

INTRODUCTION

The postseismic deformation due to great and giant earthquakes provides useful constraints on the rheological properties of rocks in subduction zones (1–7). Laboratory rock deformation experiments illustrate a stress dependency to the viscosity of rocks (8, 9), in addition to temperature, water content, and pressure dependencies. The transient and nonlinear viscous response to coseismic stress change implies a substantial reduction in the effective viscosity during the postseismic period (3, 4, 10–16). The coseismic stress changes along the plate boundary fault also drive afterslip along the plate boundary fault (6, 17–21), which is thought to occur on velocity-strengthening regions that surround velocity-weakening asperities, with a link to aftershock production (22–25). The early stages of postseismic deformation result from a combination of transient nonlinear deformation of mantle rocks (3, 4, 11, 16) and stress-driven afterslip on the fault (6, 17–21). Thus, numerical models of quasi-static deformation may provide estimates of the fault extent and viscosity structure in the subsurface.

After the 2011 M_w (moment magnitude) 9.0 Tohoku earthquake, seismogeodetic observations and modeling have illuminated the short-term dynamics of the northeastern (NE) Japan island arc subduction zone (1, 6, 16, 26–33). Often, these models have assumed no change in the rheological structure during the postseismic period and combine stress-driven relaxation based on a Maxwell or Burgers rheology with a kinematic inversion of afterslip to explain the postseismic displacement fields (1, 27–29, 31, 33), implicitly assuming no significant stress interactions between fault slip and viscoelastic flow. However, as afterslip may accrue a substantial geodetic moment, mostly aseismic, and as viscoelastic flow redistributes stress during the postseismic period, these two processes may be interacting (i.e.,

be mechanically coupled) as they diffuse the sudden stress changes imposed by the seismic cycle. The goal of this study is to assess the importance of the coupling between viscoelastic flow and afterslip and whether it constitutes a critical aspect of the postseismic relaxation.

The deformation of crust and mantle rocks, constrained by laboratory experiments on aggregates or single crystals, is accommodated by several micromechanisms that include diffusion creep, dislocation creep, dislocation glide, and Peierls creep (8, 9, 34, 35). During the steady state, i.e., at constant stress or strain rate, a constitutive relationship predicts the deformation rate based on stress and other in situ physical conditions. During periods of rapid change of stress or strain rate, other deformation processes take place within the rock, leading to a short phase of hardening that converges to the steady-state response, usually referred to as transient creep (34). In contrast to the steady state, the micromechanics of transient creep are poorly known and different constitutive relationships have been proposed (4, 36, 37), but plastic anisotropy within single crystals may be an important factor (38). Because of the rapid change imposed by the seismic cycle, transient creep may be operating during postseismic relaxation and is sometimes approximated with the linear, bi-viscous Burgers rheology (39, 40). However, Freed et al. (11, 12) and Masuti et al. (4) argue that both transient creep and power-law flow may be needed to explain the geodetic data set that they considered such that transient creep constitutes a pathway to the steady state. Following these considerations, we combine both the power-law rheology at the steady state with a power-law rheology for transient creep. We model viscoelastic relaxation with a Burgers spring-slider assembly with the following nonlinear steady-state flow law in the Maxwell element

$$\dot{\varepsilon}_M \;=\; A_M \sigma^n C_{OH}^r \exp\!\left(-\frac{Q + PV}{RT}\right) \tag{1}$$

where A_M is the pre-exponential factor, σ is the norm of the deviatoric stress tensor, n is the stress exponent, $\dot{\varepsilon}_M$ is the steady-state strain rate, Q is the activation energy, P is the pressure, V is the activation volume, R is the universal gas constant, T is the temperature, and C_{OH} and r are the water content and its exponent. The strain rate of the transient phase is represented by a deforming Kelvin element (4)

$$\dot{\varepsilon}_M \;=\; A_K \,(\sigma - 2\, G_K \varepsilon_K)^n \, C_{OH}^r \exp\!\left(-\frac{Q + PV}{RT}\right) \tag{2}$$

[1]Department of Earth Science, Tohoku University, Sendai, Japan. [2]Earth Observatory of Singapore, Nanyang Technological University, Singapore, Singapore. [3]Department of Earth Sciences, University of Southern California, Los Angeles, CA, USA. [4]Japan Agency for Marine-Earth Science and Technology, Yokohama, Japan. [5]Department of Geophysics, Tohoku University, Sendai, Japan. [6]Japan Agency for Marine-Earth Science and Technology, Yokosuka, Japan. [7]Earthquake Research Institute, The University of Tokyo, Tokyo, Japan. [8]Department of Earth and Planetary Sciences, Tokyo Institute of Technology, Tokyo, Japan.
*Corresponding author. Email: muto@tohoku.ac.jp (J.M.); james.moore@ntu.edu.sg (J.D.P.M.)

where A_K is the pre-exponential factor, G_K is the strain-hardening coefficient, and ε_K is the cumulative transient strain. We assume that the transient phase has the same sensitivity to temperature and stress as in the steady state (*34*). At the steady state before the mainshock, we assume that transient creep does not operate because of the long recurrence time between large earthquakes. Accordingly, we set $2G_K\varepsilon_K = \sigma_0$ as the initial condition, where σ_0 is a background stress of the order of 1 kPa.

Stress-driven afterslip is modeled with a velocity-strengthening friction law (*17–21*)

$$v = 2v_0 \sinh\frac{\Delta\tau}{(a-b)\,\sigma_n} \tag{3}$$

which represents a steady-state approximation of the rate-and-state friction law (*41, 42*) used to simulate all phases of the seismic cycle (*43–47*), where $\Delta\tau$ is the stress change after the mainshock,
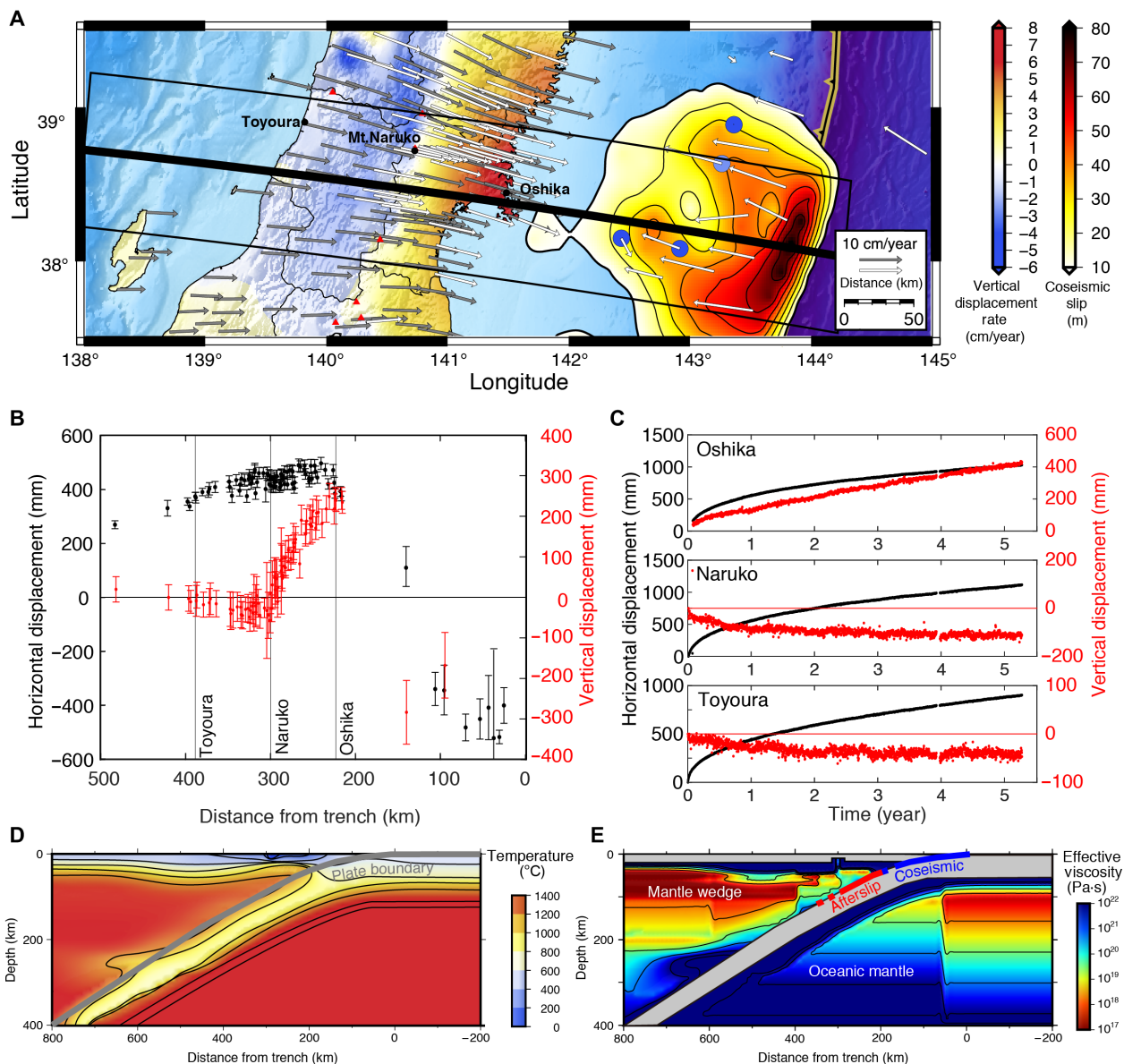

Fig. 1. Postseismic displacements recorded by land and seafloor GPS sites from September 2012 to May 2016 after the 2011 M_w 9.0 Tohoku earthquake. (**A**) Postseismic displacement field and location of the modeled transect (thick black line). Gray and white arrows indicate horizontal motions recorded by GEONET (Geospatial Information Authority of Japan) and Tohoku University/Japan Coast Guard instruments, respectively. Colors indicate vertical motions: red-blue shading for inland motion and colored circles for ocean bottom motion. Black-yellow contours in the seafloor indicate the coseismic slip distribution estimated from land and seafloor geodetic data [GPS/A; ocean bottom pressure gauge (OBP); (*14*)]. Red triangles indicate Quaternary volcanoes. Black dots indicate the site locations for time series: Oshika, Naruko, and Toyoura from east to west. (**B**) Two-dimensional displacement along the transect from September 2012 to May 2016. Black and red show horizontal and vertical displacements, respectively. (**C**) Time series of GPS displacements at the selected locations: Oshika station at the forearc, Naruko station at the volcanic front, and Toyoura station at the backarc. (**D**) Subduction zone thermal structure (*53*). (**E**) Steady-state viscosity structure calculated using the thermal structure (D).

$a - b$ is the steady-state friction parameter, σ_n is the effective normal stress on the fault accounting for the effect of pore pressure, and v represents the velocity of afterslip. Equation 3 features a non-linear response to large stress and regularization at vanishing stress compatible with linearization of the constitutive relationship (48). The numerical simulations are then performed using the integral method within the two-dimensional in-plane strain approximation using a combination of surface and volume cross-sectional elements (14, 49, 50).

Table 1. Model parameters for the postseismic deformation of the Tohoku earthquake.

	Parameter	Symbol	Value
Frictional parameters	Effective normal stress	σ_n	300 MPa
	Direct effect parameter	a	2.6×10^{-3}
	Reference slip velocity	v_o	1.9×10^{-9} m/s
Rheological parameters	Power-law exponent	n	3
	Activation energy	Q	430 kJ mol^{-1}
	Activation volume	V	13.5 cm^3 mol^{-1}
	Pre-exponential factor	A	$10^{0.56}$ s^{-1} MPa^{-n}
	Water content	C_{OH}	3100 ppm H/Si (average value in mantle wedge)
			260 ppm H/Si (average value in oceanic mantle)
	Water content exponent	r	1.2
	Prestress	σ_0	1 kPa

RESULTS

Many coastal areas in NE Japan experienced coseismic subsidence and are now undergoing postseismic uplift (Fig. 1), although they have not yet recovered to their pre-earthquake levels (51, 52). Figure 1A shows the observed 5-year postseismic displacement field (32), Fig. 1B shows the total displacements along the transect, and Fig. 1C shows the time series of displacements for the GPS stations identified in Fig. 1A. Notably, the forearc is still uplifting (e.g., Oshika station in Fig. 1C), while the subsidence along the volcanic arc and in the backarc (e.g., Naruko and Toyoura stations) has apparently ceased within the observation period (Fig. 1C).

We develop a rheology model to explain the postseismic deformation of the Tohoku earthquake over 5 years (Fig. 1), taking into account two dominant deformation mechanisms of the postseismic deformation: viscoelastic relaxation and afterslip. By comparison to the observed displacement patterns and time series, the constitutive parameters for viscoelastic flow and fault friction are determined as follows (see also Table 1). We created a thermal structure extended from (53) that includes several key characteristics of the subducting zone including a cold subducting plate and corner flow (Fig. 1D). The thermal boundary condition beneath the backarc was set on the basis of the potential temperature of 1400°C at 180-km depth in
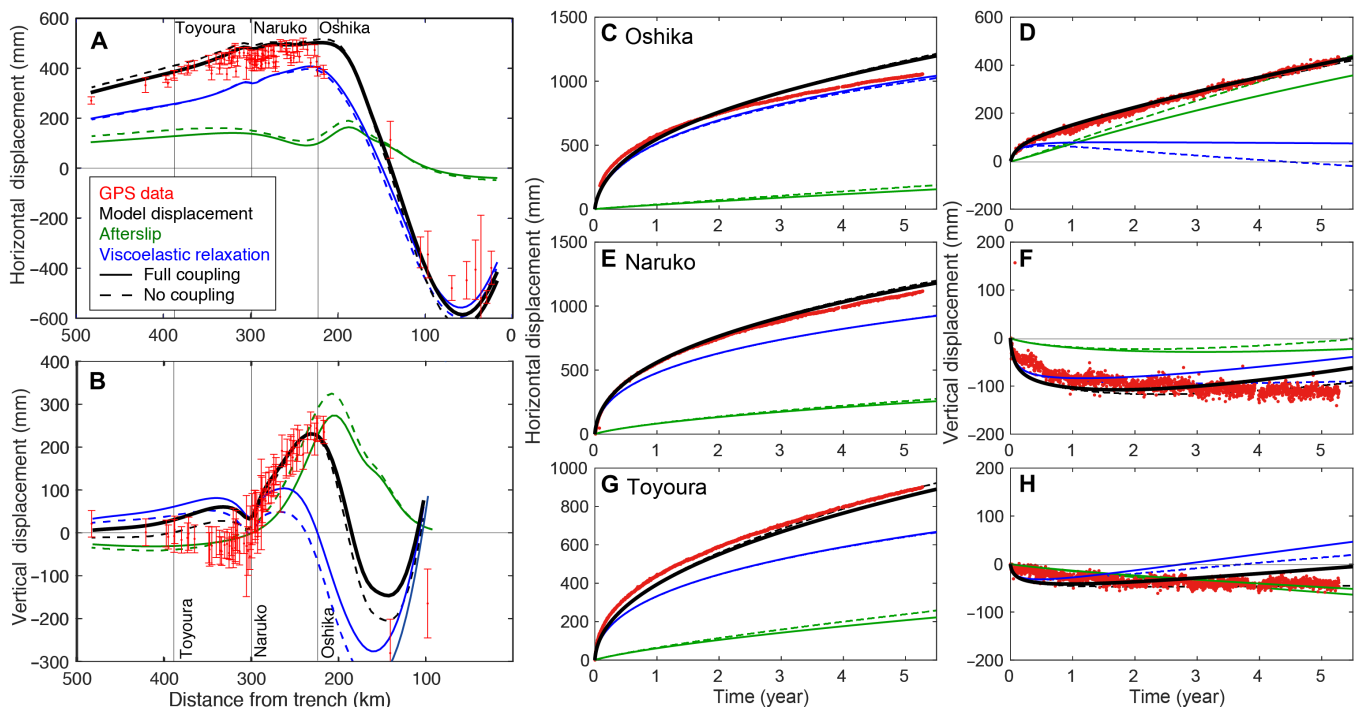

Fig. 2. Predicted postseismic deformation after the Tohoku earthquake from 2012 to 2016. (**A** and **B**) Model horizontal (A) and vertical (B) displacements (black lines) in our reference model. (**C** and **D**) Model GPS time series at Oshika station (forearc). (**E** and **F**) Model GPS time series at Naruko station (volcanic front). (**G** and **H**) Model GPS time series at Toyoura station (backarc). Red dots indicate geodetic data observed by GeoNet and Tohoku University. Blue and green lines show the component of surface deformation caused by the viscoelastic relaxation and afterslip, respectively. Solid and dashed lines show calculated displacement with and without mechanical coupling between viscoelastic relaxation and afterslip, respectively.
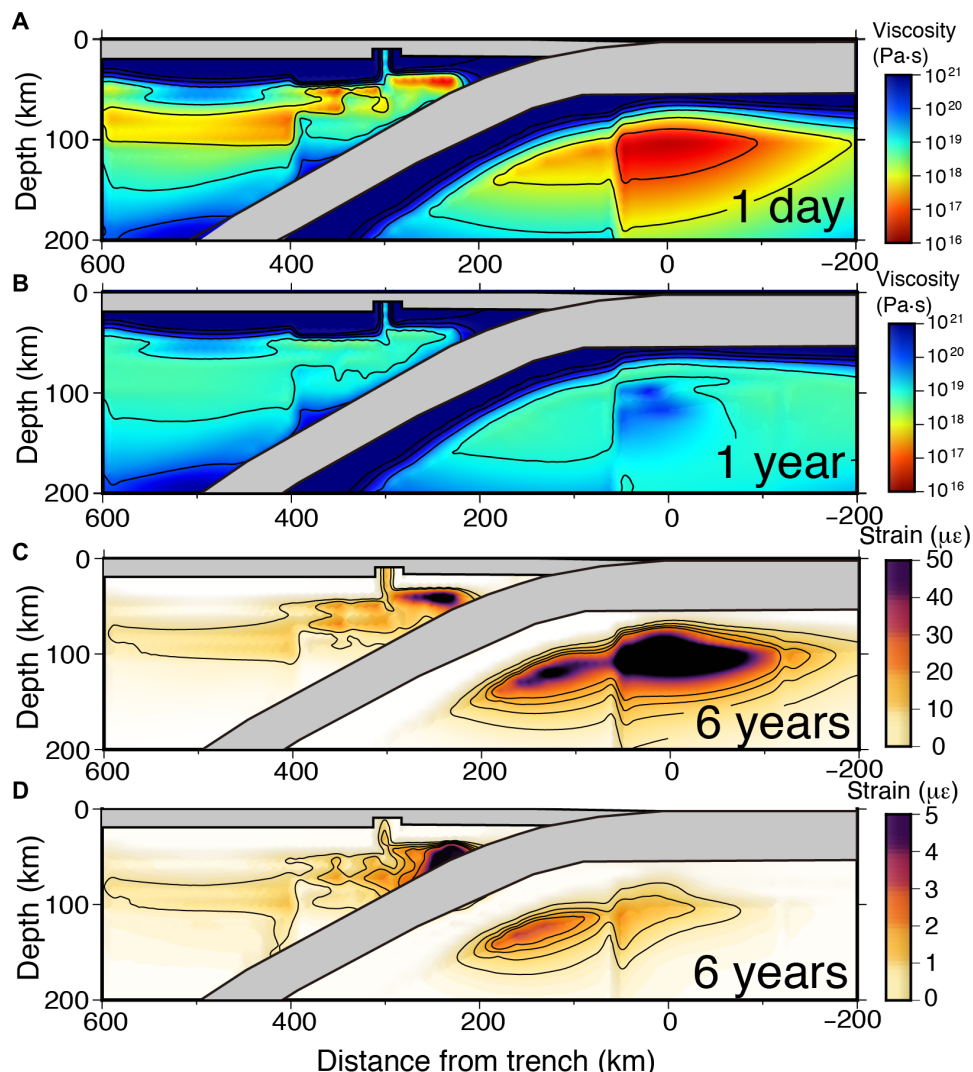
Fig. 3. Nonlinear mechanical coupling between afterslip and viscoelastic relaxation. (**A**) Effective viscosity of Kelvin element at 1 day after the mainshock. (**B**) Effective viscosity of Kelvin element at 1 year after the mainshock. (**C**) Viscous strain (second invariant of viscous strain) calculated by a fully mechanical coupled model. (**D**) Difference in strain between the model with mechanical coupling (C) and another with the coupling ignored.

mantle wedge (*53*). A preliminary sensitivity study showed that the surface deformation is not greatly sensitive to the thermal structure below 200-km depth, within reasonable bounds on the adiabatic thermal gradient. We used the laboratory-derived flow law of olivine (*8*) to calculate the steady-state viscosity with the following parameters: $Q = 430$ kJ/mol, $r = 1.2$, $n = 3$, $V = 13.5$ cm^3/mol, and the pre-exponential factor $A_M = 10^{0.56}$ s^{-1} MPa^{-n}. A recent study suggests a different sensitivity to water content of transient creep and steady-state creep, if they represent activation of different slip systems in olivine crystals (*38*). However, surface geodetic observations alone cannot distinguish the roles of water content and other prefactors independently, and lacking further constraints from laboratory experiments, we assume the same water sensitivity and prescribe $A_K = 10 A_M$, compatible with a large reduction of effective viscosity during transient creep (*11*, *39*). As the postseismic response of a nonlinear material depends on the background stress, we assumed the presence of a horizontal compressive prestress compatible with an average uniaxial strain rate across the island arc of 10^{-16} to 10^{-15}/s.

To explain the observations in detail, we assume heterogeneity in water content in the mantle wedge and the oceanic mantle. However, given the epistemic uncertainties related to the rheology of transient creep and the specific focus of the study to assess the importance of the mechanical coupling between afterslip and viscoelastic flow in the years that follow a giant earthquake, we do not place much weight on the inferred lateral variations of water content. However, the average water contents of oceanic mantle and mantle wedges are estimated to be ~260 and ~3100 parts per million (ppm) H/Si, respectively, compatible with dehydration of the oceanic mantle at spreading centers and hydration of the mantle wedge by subducted sediments and metamorphic reactions downdip from the slab. The frictional parameter of stress-driven afterslip was constrained in particular by the surface vertical motion. Data are best explained by a frictional parameter of $(a - b)\sigma \sim 0.8$ MPa and $V_0 = 1.9 \times 10^{-9}$ m/s throughout the downdip extension of the main rupture region.

The combination of a power-law rheology for distributed deformation with velocity-strengthening stress-driven afterslip on
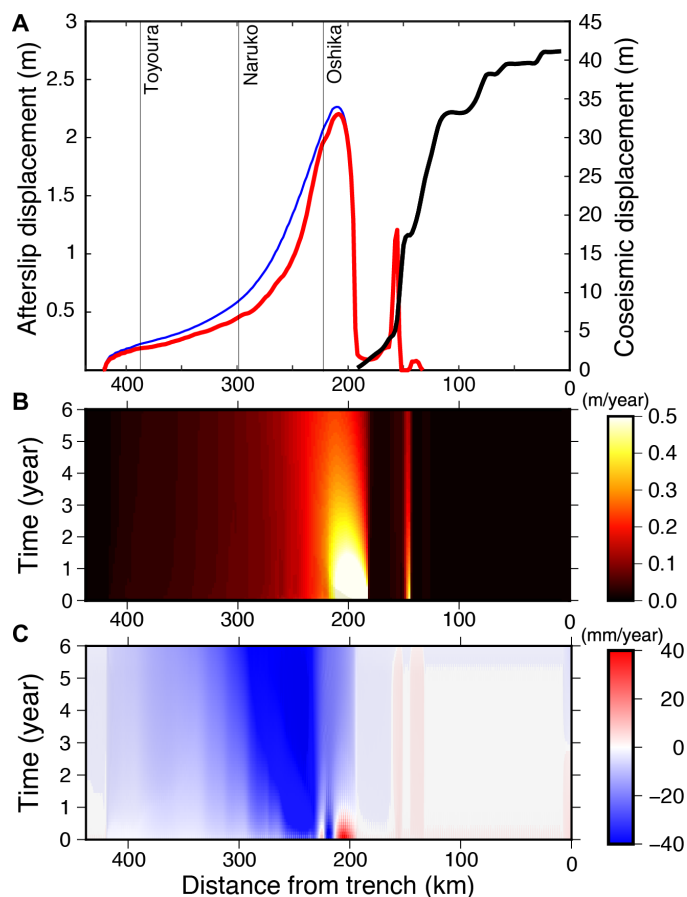
Fig. 4. Afterslip distribution and effect of mechanical coupling. (**A**) Estimates of afterslip distribution using the reference model and coseismic slip distribution (*35*). Red and blue lines show estimates with and without mechanical coupling between viscoelastic relaxation and afterslip, respectively. Black line shows the coseismic slip distribution used in the model (right axis). (**B**) Afterslip rate with time in the coupling model. (**C**) Difference in afterslip rates between the model with mechanical coupling (B) and another with the coupling ignored: Difference = Coupling − Noncoupling.

the plate interface explains the total observed two-dimensional horizontal (Fig. 2A) and vertical (Fig. 2B) displacement fields well. The horizontal displacement is dominated by viscoelastic relaxation. However, the vertical deformation is more sensitive to rheological heterogeneities. In some regions, the surface displacements caused by afterslip and viscoelastic relaxation may have the opposite sense, in particular the vertical motion in the forearc region (Fig. 2B). In those regions, deeper viscoelastic relaxation results in subsidence, while shallower afterslip drives uplift in the 5-year period. In general, these results are compatible with previous studies (*6, 29*).

Figure 2 (C to H) illustrates the GPS time series of selected locations across the NE Japan arc (site locations in Fig. 1A). With a similar spatial variation as the observed displacement, viscoelastic relaxation dominates the horizontal component of the time series at almost all locations. On the other hand, opposite contributions of both mechanisms can be seen in the time series of vertical deformation: Afterslip drives steady uplift, and viscoelastic relaxation results in subsidence at the forearc (Oshika station in Fig. 2D). In particular, the contribution of afterslip is large in the forearc region close to the source area and becomes smaller with distance from the source. Additionally, for both components of displacement, the time dependence is different for the two mechanisms: Viscoelastic deformation is initially rapid because of the transient and nonlinear response but decays with time according to temporal changes in effective viscosity driven by the coseismic stress change (Fig. 3, A and B, and figs. S4 and S5).

Figure 4 shows the afterslip distribution at 5 years after the coseismic event. The afterslip mainly occurs at the region directly downdip of the main rupture area, where coseismic stress changes are large (depth of ~30 km; figs. S1 and S2). We find a peak afterslip after 5 years of ~2.5 m and a slip rate (average rate of ~0.5 m/year in 5 years; Fig. 4A), consistent with some previous estimates from the early postseismic observations (*28, 29*). The second sharp peak in afterslip at the 180-km distance from the trench is likely driven by large gradients in coseismic slip associated with local stress concentration.

DISCUSSION
Although the afterslip rate gradually decreases with time in the 5 years of the postseismic period (Fig. 4B), it causes persistent uplift in the
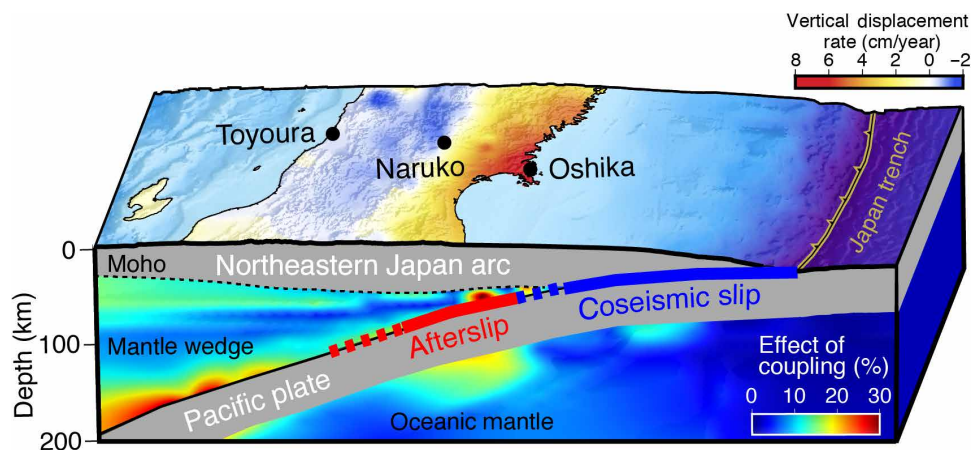

Fig. 5. Schematic of mechanical coupling between viscoelastic relaxation and afterslip. Contours show the relative importance of mechanical coupling (%) on subsurface deformation after 6 years. The effect of coupling is calculated by the ratio of the difference in strain between the coupled and uncoupled models to the total strain in the mechanically coupled model. Coupling between viscoelastic flow and afterslip is the most important at the downdip of the mainshock below the coastline.

coseismically subsided coastal area (Fig. 2). The lack of deep afterslip in the postseismic deformation of the Tohoku earthquake had previously been inferred (33) from 5 years of GPS horizontal motion. The difference in results between these analyses may be due to the continuation of stress-driven afterslip embedded in a material deforming with a power-law rheology. Strong viscosity reduction and mechanical coupling causes continuous loading of the plate boundary fault driving persistent afterslip directly downdip of the main rupture (Fig. 3A and figs. S4 and S5).

Equipped with a reference model that fits 5 years of geodetic observations, we may now discuss the importance of the mechanical coupling between afterslip and viscoelastic flow. Here, the coupling allows two different interactions: viscoelastic flow triggered by the occurrence of afterslip (afterslip to viscoelastic relaxation = AV coupling) and persistent afterslip influenced by viscoelastic flow (= VA coupling). The details of the coupling depend on the geometry of the viscoelastic materials and the megathrust, but for the NE Japan subduction zone, we find that neglecting the mechanical interaction between viscoelastic flow and afterslip on the plate boundary fault introduces a variance of up to 25% (Fig. 4A) on the amplitude of afterslip below the coast (around 70- to 80-km depth). The difference in afterslip rate by the coupling reaches up to half of the steady-state subduction rate (Fig. 4C) and can alter the surface displacements (dashed lines in Fig. 2 and fig. S3). Only allowing changes in tractions on the plate boundary fault due to viscoelastic flow (VA coupling) decreases the afterslip amount at around 70- to 100-km depth. This is close to the region where the viscosity of the mantle wedge is decreased by the coseismic stress change (e.g., Fig. 3, A and B, and figs. S4 and S5), indicating that viscoelastic flow in this region effectively relaxes the stress on the plate boundary fault. Conversely, the viscoelastic flow loads the fault at around 50- to 80-km depth, driving persistent afterslip (Fig. 4). Notably, only allowing the stress on viscoelastic materials caused by afterslip (AV coupling) results in more vertical deformation (i.e., uplift) in the coastal regions (dotted line in fig. S3B). This is due to the stress on the plate boundary that can only be relaxed by afterslip, not being damped by the global viscoelastic relaxation (VA coupling) occurring in mantle wedges and oceanic mantle, and causing a stress-driven afterslip directly downdip of the main rupture.

The effect of mechanical coupling is most important in the region directly downdip of the main rupture in the forearc mantle wedge (Fig. 5), where the effective viscosity was greatly reduced in the transient phase by the large stress perturbation from the mainshock (Fig. 3, A and B). The importance of coupling grows as the postseismic transient develops, and up to 15% of viscous strain in mantle wedge over 5 years is caused by the afterslip via this coupling (Fig. 3, C and D). It is smaller in the early phase of the postseismic deformation and may, in some cases, be neglected during this period (time series in Fig. 2 and fig. S3). However, the coupling becomes more pronounced with time. Eventually, the coupling drives 20 to 30% of the total strain at the downdip region of the main rupture (Fig. 5). Substantial differences in the postseismic uplift on the order of ~10 cm might occur at the coastal regions over 5 years (fig. S3B). Thus, we highlight the importance of addressing mechanical coupling for long-term studies of postseismic relaxation, in particular when combining kinematic inversion with forward models for viscoelastic relaxation, where estimates of the recovery of plate coupling and postseismic uplift may be significantly modified. Incorporating the constitutive rock behavior constrained by mineral physics and in-cluding the mechanical coupling between localized and distributed deformation may be key to better predict the future recovery of the coseismically subsided coastal area through postseismic uplift and quantify the seismic hazards of inland faults with the progress of the postseismic deformation.

MATERIALS AND METHODS
Numerical model
We developed a two-dimensional model to explain the postseismic deformation of the Tohoku earthquake over 5 years (Fig. 1). The simulation was performed using the integral method in the condition of in-plane strain (14, 49, 50). We calculated the stress interactions among the embedded surface and volume elements with analytic solutions for both displacements and distributed strain caused by viscoelastic deformation of a finite cross-sectional area. The evolution of stress, slip rate, strain rate, and the frictional state parameter was then solved numerically throughout the postseismic period using the integral method.

The simplification of the model introduced by the two-dimensional approximation allows us to explore a realistic rheology for the NE Japan subduction zone compatible with mineral physics and to explain the wealth of geodetic observations. Following a previous study (29), we construct a two-dimensional transect (black line in Fig. 1A) normal to the trench axis around the Miyagi-Yamagata area in the central part of NE Japan, where the peak coseismic slip was observed (54). The coseismic slip distribution calculated along the transect based on a three-dimensional coseismic slip distribution by (54) in a previous study (29) was used. The model covers 800 km to the west and 200 km to the east from the trench with 400-km depth. We considered slip on the plate boundary fault (patch width of 2 km) and distributed viscoelastic deformation of the surrounding inland lower crust, mantle wedge, and oceanic mantle (rectangular areas of 5 km × 5 km).

The steady-state viscosity (Fig. 1E) was estimated from the laboratory-derived flow laws of olivine (8). We included spatial variations in viscosity due to the temperature-dependent rheology obtained from a subduction zone thermal flow model (Fig. 1D) (53). The thermal model from (53) only covered 600 km west from the trench, so we extended it to 800 km by solving a one-dimensional half-space cooling model. Thermal structure beneath the oceanic lithosphere was created according to (55) and combined into the thermal model of the island arc by (53). The steady-state viscosity (Fig. 1E) was estimated using the thermal structure with heterogeneous water distribution. The viscosity structure also includes notable effects from the weak volcanic front and strong forearc (cold nose) based on the results of previous studies (1, 29, 31). We searched the following optimum ranges of water contents to explain the observations: average water contents of 260 and 3100 ppm H/Si for oceanic mantle and mantle wedge, respectively. The former is consistent with a previous estimate of the viscosity structure of the oceanic mantle from the early postseismic deformation of the 2011 Tohoku earthquake (29).

We modeled afterslip using the regularized rate-strengthening approximation of the rate-and-state–dependent friction law (17–21). Afterslip is not allowed in fault regions of negative coseismic stress change. Plate boundary was modeled by shallow coseismic slip region and deep afterslip region. We explored the values of reference slip velocity V_0 and $(a - b)\sigma$ values in Eq. 3 that best explain the

geodetic observations in combination with viscoelastic relaxation under the stable subduction of the Pacific plate (8 cm/year). In particular, afterslip location at the downdip region of the main rupture can be constrained by comparison to the vertical motion at the forearc (e.g., Oshika station).

Geodetic observation

For the postseismic deformation of the 2011 Tohoku earthquake, we incorporated observations from continuous GPS stations on land deployed by the Geospatial Information Authority of Japan (GEONET, gray arrows in Fig. 1A) and Tohoku University as well as seafloor observations deployed by Japan Coast Guard and Tohoku University (white arrows) (14). In the 6 years of the postseismic period, dense and wide GPS-A observation network was constructed along the Japan trench in September 2012 and six campaign surveys were conducted at most site until May 2016 (32). Accumulated postseismic displacements were calculated for the period. The displacements for both the on-land GPS and seafloor GPS-A data were estimated relative to the North American plate. We did not correct the effect of interplate coupling during the period because we could not obtain the pre-earthquake deformation rate for the seafloor observations that was installed after the earthquake.

SUPPLEMENTARY MATERIALS

Supplementary material for this article is available at http://advances.sciencemag.org/cgi/content/full/5/9/eaaw1164/DC1

Fig. S1. Coseismic stress change calculated by the coseismic slip model of (20).
Fig. S2. Stress change caused by cumulative afterslip at 6 years after the 2011 Tohoku earthquake in a fully mechanical coupling model.
Fig. S3. Effect of mechanical coupling on the GPS time series.
Fig. S4. Temporal change in effective viscosities of the Kelvin element within the Burgers rheology.
Fig. S5. Temporal change in effective viscosities of Maxwell medium in Burgers rheology.

REFERENCES AND NOTES

1. T. Sun, K. Wang, T. Iinuma, R. Hino, J. He, H. Fujimoto, M. Kido, Y. Osada, S. Miura, Y. Ohta, Y. Hu, Prevalence of viscoelastic relaxation after the 2011 Tohoku-Oki earthquake. *Nature* **514**, 84–87 (2014).
2. K. Wang, Y. Hu, J. He, Deformation cycles of subduction earthquakes in a viscoelastic Earth. *Nature* **484**, 327–332 (2012).
3. Q. Qiu, J. D. P. Moore, S. Barbot, L. Feng, E. M. Hill, Transient rheology of the Sumatran mantle wedge revealed by a decade of great earthquakes. *Nat. Commun.* **9**, 995 (2018).
4. S. Masuti, S. D. Barbot, S.-i. Karato, L. Feng, P. Banerjee, Upper-mantle water stratification inferred from observations of the 2012 Indian Ocean earthquake. *Nature* **538**, 373–377 (2016).
5. Y. Hu, R. Bürgmann, P. Banerjee, L. Feng, E. M. Hill, T. Ito, T. Tabei, K. Wang, Asthenosphere rheology inferred from observations of the 2012 Indian Ocean Earthquake. *Nature* **538**, 368–372 (2016).
6. Y. Hu, R. Bürgmann, N. Uchida, P. Banerjee, J. T. Freymueller, Stress-driven relaxation of heterogeneous upper mantle and time-dependent afterslip following the 2011 Tohoku earthquake. *J. Geophys. Res.* **121**, 385–411 (2016).
7. H. Suito, J. T. Freymueller, A viscoelastic and afterslip postseismic deformation model for the 1964 Alaska earthquake. *J. Geophys. Res.* **114**, B11404 (2009).
8. S.-i. Karato, H. Jung, Effects of pressure on high-temperature dislocation creep in olivine. *Philos. Mag.* **83**, 401–414 (2003).
9. R. Bürgmann, G. Dresen, Rheology of the lower crust and upper mantle: Evidence from rock mechanics, geodesy, and field observations. *Annu. Rev. Earth Planet. Sci.* **36**, 531–567 (2008).
10. A. M. Freed, R. Bürgmann, Evidence of power-law flow in the Mojave desert mantle. *Nature* **430**, 548–551 (2004).
11. A. M. Freed, G. Hirth, M. D. Behn, Using short-term postseismic displacements to infer the ambient deformation conditions of the upper mantle. *J. Geophys. Res.* **117**, B01409 (2011).
12. A. M. Freed, T. Herring, R. Bürgmann, Steady-state laboratory flow laws alone fail to explain postseismic observations. *Earth Planet. Sci. Lett.* **300**, 1–10 (2010).
13. J. D. P. Moore, H. Yu, C.-H. Tang, T. Wang, S. Barbot, D. Peng, S. Masuti, J. Dauwels, Y.-J. Hsu, V. Lambert, P. Nanjundiah, S. Wei, E. Lindsey, L. Feng, B. Shibazaki,

14. S. Barbot, Asthenosphere flow modulated by megathrust earthquake cycles. *Geophys. Res. Lett.* **45**, 6018–6031 (2018).
15. C. H. Tang, Y.-J. Hsu, S. Barbot, J. D. P. Moore, W.-L. Chang, Lower-crustal rheology and thermal gradient in the Taiwan orogenic belt illuminated by the 1999 Chi-Chi earthquake. *Sci. Adv.* **5**, eaav3287 (2019).
16. R. Agata, S. D. Barbot, K. Fujita, M. Hyodo, T. Iinuma, R. Nakata, T. Ichimura, T. Hori, Rapid mantle flow with power-law creep explains deformation after the 2011 Tohoku mega-quake. *Nat. Commun.* **10**, 1385 (2019).
17. K. M. Johnson, R. Bürgmann, K. Larson, Frictional properties on the San Andreas Fault near Parfkfield, California, inferred from models of afterslip following the 2004 earthquake. *Bull. Seismol. Soc. Am.* **96**, S321–S338 (2006).
18. H. Perfettini, J.-P. Avouac, Modeling afterslip and aftershocks following the 1992 Landers earthquake. *J. Geophys. Res. Solid Earth* **112**, B07409 (2007).
19. S. Barbot, Y. Fialko, Y. Bock, Postseismic deformation due to the M_w 6.0 2004 Parkfield earthquake: Stress-driven creep on a fault with spatially variable rate-and-state friction parameters. *J. Geophys. Res. Solid Earth* **114**, B07405 (2009).
20. B. Rousset, S. Barbot, J.-P. Avouac, Y.-J. Hsu, Postseismic deformation following the 1999 Chi-Chi earthquake, Taiwan: Implication for lower-crust rheology. *J. Geophys. Res. Solid Earth* **117**, B12405 (2012).
21. C. Rollins, S. Barbot, J.-P. Avouac, Postseismic deformation following the 2010 M = 7.2 El Mayor-Cucapah earthquake: Observations, kinematic inversions, and dynamic models. *Pure Appl. Geophys.* **172**, 1305–1358 (2015).
22. H. Perfettini, J. P. Ampuero, Dynamics of a velocity strengthening fault region: Implications for slow earthquakes and postseismic slip. *J. Geophys. Res. Solid Earth* **113**, B09411 (2008).
23. H. Perfettini, J.-P. Avouac, H. Tavera, A. Kositsky, J.-M. Nocquet, F. Bondoux, M. Chlieh, A. Sladen, L. Audin, D. L. Farber, P. Soler, Seismic and aseismic slip on the Central Peru megathrust. *Nature* **465**, 78–81 (2010).
24. W. B. Frank, P. Poli, H. Perfettini, Mapping the rheology of the Central Chile subduction zone with aftershocks. *Geophys. Res. Lett.* **44**, 5374–5382 (2017).
25. H. Perfettini, W. B. Frank, D. Marsan, M. Bouchon, A model of aftershock migration driven by afterslip. *Geophys. Res. Lett.* **45**, 2283–2293 (2018).
26. M. Simons, S. E. Minson, A. Sladen, F. Ortega, J. Jiang, S. E. Owen, L. Meng, J.-P. Ampuero, S. Wei, R. Chu, D. V. Helmberger, H. Kanamori, E. Hetland, A. W. Moore, F. H. Webb, The 2011 magnitude 9.0 Tohoku-oki earthquake: Mosaicking the megathrust from seconds to centuries. *Science* **332**, 1421–1425 (2011).
27. S. Yamagiwa, S. Miyazaki, K. Hirahara, Y. Fukahata, Afterslip and viscoelastic relaxation following the 2011 Tohoku-oki earthquake (M_w9.0) inferred from inland GPS and seafloor GPS/Acoustic data. *Geophys. Res. Lett.* **42**, 66–73 (2015).
28. T. Iinuma, R. Hino, N. Uchida, W. Nakamura, M. Kido, Y. Osada, S. Miura, Seafloor observations indicate spatial separation of coseismic and postseismic slips in the 2011 Tohoku earthquake. *Nat. Commun.* **7**, 13506 (2016).
29. J. Muto, B. Shibazaki, T. Iinuma, Y. Ito, Y. Ohta, S. Miura, Y. Nakai, Heterogeneous rheology controlled postseismic deformation of the 2011 Tohoku-Oki earthquake. *Geophys. Res. Lett.* **43**, 4971–4978 (2016).
30. N. Uchida, T. Iinuma, R. M. Nadeau, R. Bürgmann, R. Hino, Periodic slow slip triggers megathrust zone earthquakes in northeastern Japan. *Science* **351**, 488–492 (2016).
31. A. M. Freed, A. Hashima, T. W. Becker, D. A. Okaya, H. Sato, Y. Hatanaka, Resolving depth-dependent subduction zone viscosity and afterslip from postseismic displacements following the 2011 Tohoku-Oki, Japan earthquake. *Earth Planet. Sci. Lett.* **459**, 279–290 (2017).
32. T. Tomita, M. Kido, Y. Ohta, T. Iinuma, R. Hino, Along-trench variation in seafloor displacements after the 2011 Tohoku earthquake. *Sci. Adv.* **3**, e1700113 (2017).
33. K. Wang, T. Sun, L. Brown, R. Hino, F. Tomita, M. Kido, T. Iinuma, S. Kodaira, T. Fujiwara, Learning from crustal deformation associated with M9 2011 Tohoku-oki earthquake. *Geosphere* **14**, 552–571 (2018).
34. P. Chopra, High-temperature transient creep in olivine rocks. *Tectonophysics* **279**, 93–111 (1997).
35. G. Hirth, D. L. Kohlstedt, Rheology of the upper mantle and the mantle wedge: A view from the experimentalists, in *The Subduction Factory: Geophysical Monograph Series*, J. Eiler, Ed. (Blackwell Publishing Ltd., 2003), vol. 138, pp. 83–102.
36. M. Thieme, S. Demouchy, D. Mainprice, F. Barou, P. Cordier, Stress evolution and associated microstructure during transient creep of olivine at 1000–1200° C. *Phys. Earth Planet. Inter.* **278**, 34–46 (2018).
37. B. K. Holtzman, A. Chrysochoos, L. Daridon, A thermomechanical framework for analysis of microstructural evolution: Application to olivine rocks at high temperature. *J. Geophys. Res. Solid Earth* **123**, 8474–8507 (2018).
38. S. Masuti, S.-i. Karato, J. Girard, S. Barbot, Anisotropic high-temperature creep in hydrous oli.vine single crystals and its geodynamic implications. *Phys. Earth Planet. Inter.* **290**, 1–9 (2019).

39. F. Pollitz, P. Banerjee, K. Grijalva, B. Nagarajan, R. Bürgmann, Effect of 3-D viscoelastic structure on post-seismic relaxation from the 2004 M = 9.2 Sumatra earthquake. *Geophys. J. Int.* **173**, 189–204 (2008).

40. A. Hoechner, S. V. Sobolev, I. Einarsson, R. Wang, Investigation on afterslip and steady state and transient rheology based on postseismic deformation and geoid change caused by the Sumatra 2004 earthquake. *Geochem. Geophys. Geosyst.* **12**, Q07010 (2011).

41. A. Ruina, Slip instability and state variable friction laws. *J. Geophys. Res. Solid Earth* **88**, 10359–10370 (1983).

42. J. H. Dieterich, Modeling of rock friction: 1. Experimental results and constitutive equations. *J. Geophys. Res. Solid Earth* **84**, 2161–2168 (1979).

43. J. R. Rice, S. T. Tse, Dynamic motion of a single degree of freedom system following a rate and state dependent friction law. *J. Geophys. Res. Solid Earth* **91**, 521–530 (1986).

44. N. Lapusta, J. R. Rice, Y. Ben-Zion, G. Zheng, Elastodynamic analysis for slow tectonic loading with spontaneous rupture episodes on faults with rate-and state-dependent friction. *J. Geophys. Res. Solid Earth* **105**, 23765–23789 (2000).

45. S. Barbot, N. Lapusta, J. P. Avouac, Under the hood of the earthquake machine: Toward predictive modeling of the seismic cycle. *Science* **336**, 707–710 (2012).

46. N. Lapusta, S. Barbot, Models of earthquakes and aseismic slip based on laboratory-derived rate and state friction laws, in *The Mechanics of Faulting: From Laboratory to Real Earthquakes*, A. Bizzari, H. S. Bhat Eds. (Earth Observatory of Singapore, 2012), pp. 153–207.

47. D. M. Veedu, S. Barbot, The Parkfield tremors reveal slow and fast ruptures on the same asperity. *Nature* **532**, 361–365 (2016).

48. R. C. Viesca, P. Dublanchet, The slow slip of viscous faults. *J. Geophys. Res. Solid Earth* **124**, 4959–4983 (2019).

49. V. Lambert, S. Barbot, Contribution of viscoelastic flow in earthquake cycles within the lithosphere-asthenosphere system. *Geophys. Res. Lett.* **43**, 10142–10154 (2016).

50. S. Barbot, J. D. P. Moore, V. Lambert, Displacement and stress associated with distributed anelastic deformation in a half-space. *Bull. Seismol. Soc. Am.* **107**, 821–855 (2017).

51. M. Tobita, Combined logarithmic and exponential function model for fitting postseismic GNSS time series after 2011 Tohoku-Oki earthquake. *Earth Planet. Space* **68**, 41 (2016).

52. T. Iinuma, Postseismic uplift along the pacific coast of Tohoku and Kanto districts associated with the 2011 off the Pacific Coast of Tohoku Earthquake. *J. Des. Res.* **13**, 48805 (2017).

53. S.-s. Horiuchi, H. Iwamori, A consistent model for fluid distribution, viscosity distribution, and flow-thermal structure in subduction zone. *J. Geophys. Res.* **121**, 3238–3260 (2016).

54. T. Iinuma, R. Hino, M. Kido, D. Inazu, Y. Osada, Y. Ito, M. Ohzono, H. Tsushima, S. Suzuki, H. Fujimoto, S. Miura, Coseismic slip distribution of the 2011 off the Pacific Coast of Tohoku Earthquake (M9.0) refined by means of seafloor geodetic data. *J. Geophys. Res.* **117**, B07409 (2012).

55. E. M. Syracuse, P. E. van Keken, G. A. Abers, The global range of subduction zone thermal models. *Phys. Earth Planet. Inter.* **183**, 73–90 (2010).

Citation: J. Muto, J. D. P. Moore, S. Barbot, T. Iinuma, Y. Ohta, H. Iwamori, Coupled afterslip and transient mantle flow after the 2011 Tohoku earthquake. *Sci. Adv.* **5**, eaaw1164 (2019).